Organic & Biomolecular Chemistry

Accepted Manuscript

ROYAL SOCIETY OF CHEMISTRY

www.rsc.org/obc

Journal Name

RSCPublishing

ARTICLE

Cross-strand histidine-aromatic interactions enhance acyl-transfer rates in beta-hairpin peptide catalysts

Cite this: DOI: 10.1039/xoxxoooooox

M. Matsumoto,[a] S. J. Lee,[b] M. R. Gagné,[a]* and M. L. Waters [a]*

Received ooth January 2012,
Accepted ooth January 2012

DOI: 10.1039/xoxxoooooox

www.rsc.org/

A reactive tagging methodology was used to select the species most reactive to an acylation reagent from a solid phase library of beta hairpin peptides. Hits bearing an electron-rich aromatic residue across strand from a reactive histidine were found to competitively become *N*-acylated. In addition to displaying rapid *N*-acylation rates the hit peptide was additionally deacylated in the presence of a nucleophile, thus closing a putative catalytic cycle. Variants of the hit peptide were studied to elucidate both the magnitude (up to 18,000-fold over background, k_{cat}/k_{uncat} = 94,000,000, or 45-fold over Boc-histidine methyl ester) and mechanism of acyl transfer catalysis. A combination of CH-π, cation-π and $HisH^+$-O interactions in the cationic imidazole transition state is implicated in the rate acceleration, in addition to the fidelity of the beta hairpin fold. Moreover, NMR structural data on key intermediates or models thereof suggest that a key feature of this catalyst is the ability to access several different stabilizing conformations along the catalysis reaction coordinate.

Background

The *de novo* design of biomimetic catalysts remains a challenge for applications in synthetic chemistry. To begin understanding how enzymes achieve their unrivalled rate accelerations and selectivity, synthetic chemists have made great efforts to construct systems that mimic selected aspects of their natural counterparts.[1] Recent directions include selection based approaches that are a viable alternative to the resource-intensive classic cycle of design, synthesis, evaluation, and redesign.[2] The development of peptide-based biomimetic catalysts has also been enabled by solid phase peptide synthesis (SPPS), which makes accessible a wide range of short to medium length peptides.[3] SPPS is efficient enough to create small libraries of peptides that can be screened on bead for functional properties, taking advantage of peptide modularity, sequence-dependent secondary structure, and valuable structural and functional precedents from biology. Peptide organocatalysis[4] has additionally paved the way for the study of structure/ reactivity relationships in organic solvents, which avoids the problems associated with achieving stable structures in water. Non-aqueous peptide catalysis thus provides a "blank canvas" on which to explore the effect of inter-residue interactions on reactivity.

We have previously described the discovery and characterization of high-activity acyl transfer catalysts identified via reactive tagging of on-bead libraries of helical peptides. The reactive tagging technique uses dye-appended substrates that, in the absence of a nucleophile, can covalently tag the most reactive imidazole sidechain present in a library of histidine (His)-containing peptides (Scheme 1). This method has previously identified high activity helical[5] peptides for acyl transfer catalysis with a preference for aromatic residues near the catalytic His. The accelerating role of His-aromatic pairs is not obvious despite having been selected our previously described helical libraries. Herein we detail the identification and characterization of catalytic β-hairpins, which also utilize His-aromatic interactions, as well as mechanistic and structural studies investigating the role for His-pi interactions in catalysis.

Scheme 1. Deprotonation of the acylimidazolium intermediate leads to catalyst trapping as a neutral *N*-acyl imidazole.

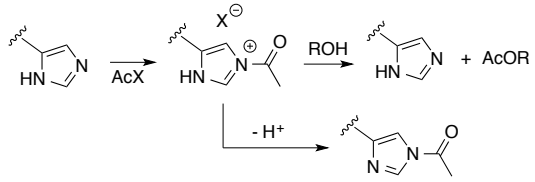

The kinetic benefit of a close association between His and an aromatic group in helical peptide catalysts led us to screen a focused library of beta-hairpin peptides that position variable aromatic (and also hydrogen-bonding) residues in close proximity to the catalytic histidine. As will be discussed, this study clearly demonstrates that properly positioned aromatic residues can significantly enhance the catalytic activity of His-containing catalysts. The data show the criticality of proper hairpin folding to catalytic function, but also that high activities are reliant on specific, but flexible, noncovalent interactions between the His and aromatic sidechain of the beta hairpin.

Results

Library design

To produce structurally discrete, well-organized catalysts with the sought after stabilizing close contacts, we chose to assemble libraries wherein the catalytic site (His) is localized within a beta-hairpin peptide. Since the sidechains alternate in a beta-sheet, they create two faces: the hydrogen bonded (HB) face, consisting of sidechains from residues that form cross-strand hydrogen bonds, and the non-hydrogen bonded (NHB) face, which consists of residues whose H-bond functionality point away from the interface. Since His units are a conserved residue in acyl transfer enzyme active sites (nucleophile or base),[6] our design positions such a site on the NHB face of the beta hairpin as this face provides more conformational freedom than the HB face. The cross-strand sidechains additionally interdigitate such that the His residue located at position 9 in our test structure is flanked by its cross-strand partner at position 4 (z in Figure 1) and its diagonal partner at position 2 (x in Figure 1).[7] These design elements are well supported by a wealth of structural information on beta-hairpins, both in organic and aqueous solvents.[8,9,10] To provide a diverse set of mechanistically inspired variable residues at these positions, a combination of aromatic and hydrogen bond donor/acceptor groups were included as the former were found to be beneficial in a number of helical and beta-hairpin peptide catalysts,[5] while the latter could help stabilize positive or negative charge buildup in the transition state. Valine was also included because it stabilizes the beta-hairpin structure. The remaining residues were held constant and were selected to provide a well-folded organic-soluble beta hairpin,[9] with beta-branched aliphatic amino acids in the strands, and a beta-hairpin nucleating dPro-Gly turn sequence.[11]

Library synthesis and screening

A solid phase library of 100 12-residue peptides was synthesized using split-and-mix methodology[12] on Tentagel S-NH_2 incorporating a photolabile nitroveratryl linker,[13] with a dPro-Gly turn sequence at positions 6 and 7,[11] and variable residues located at positions 2 and 4 that flank the position 9 histidine (Figure 1). The resulting on-bead library was screened with dye-tagged nitrophenyl ester **1** in dichloromethane (DCM).[14] Under these competitive His-acylation conditions, those catalysts possessing a kinetic advantage should preferentially generate the *N*-acyl imidazole intermediate that dye tags the structure.

Incubating the library with a 10 mM solution of **1** in DCM for 1 hour led to <5% of the beads becoming visibly more colored (red) than the remainder. These more reactive beads were separated under a dissecting microscope and subjected to photocleavage in methanol (which decolorizes the beads) under a 360 nm UV lamp. The peptides identified by MALDI-FTMS from these colored beads are those more capable of forming the N-acyl intermediate and thus constitute good leads for catalyst development. Analysis of this 100-component library revealed

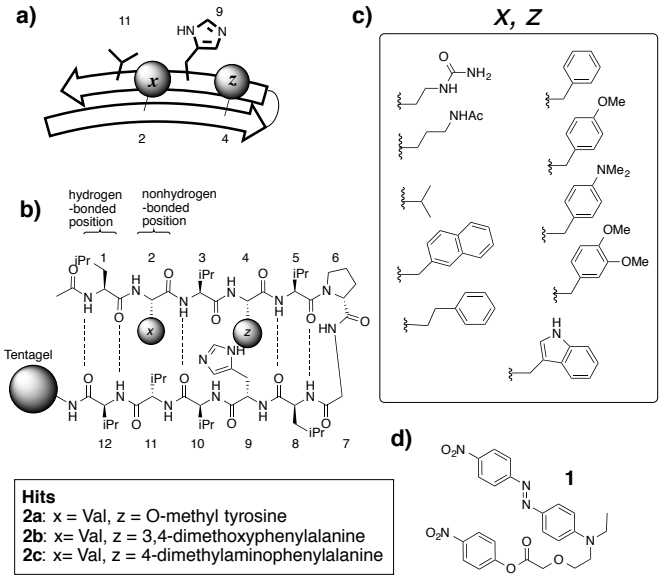

Figure 1. (a) Cartoon representation of beta-hairpin showing the interdigitating nature of the sidechain on the non-H-bonding face; (b) sequence of the beta-hairpins in the library screen; (c) Sidechains included in the library at positions X and Z; (d) Tag **1**.

that each hit contained a completely conserved valine residue at position 2. Position 4 was more variable and found to be populated by aromatic residues containing heteroatoms; O-methyltyrosine, MeY, (**2a**) was major and 3,4-dimethoxyphenylalanine (**2b**) and 4-dimethylamino phenylalanine (**2c**) were minor (Figure 1).

The top candidate peptide **2a** was resynthesized by

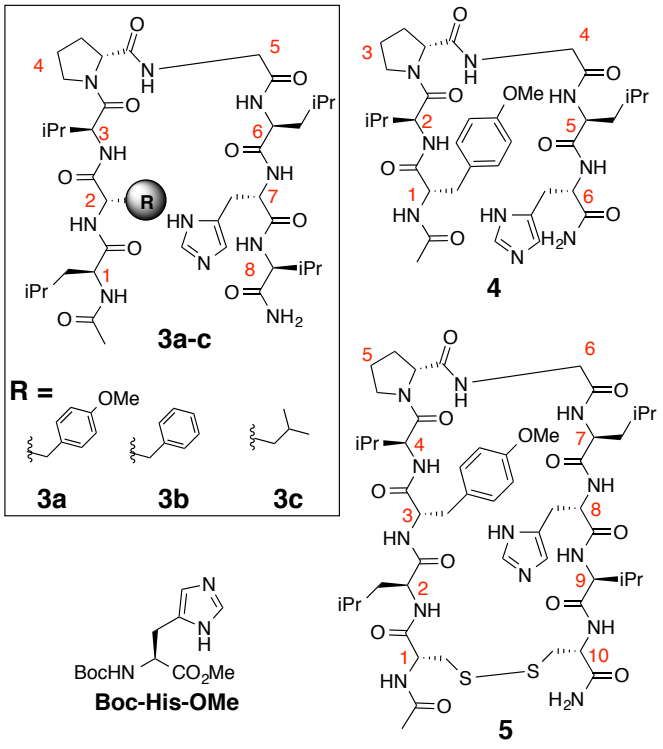

Figure 2. Beta hairpin peptide derivatives investigated in this study. 8-mer **3a-c**; 6-mer **4;** and cyclic disulfide **5**.

conventional solution methodologies, but was unfortunately prone to aggregation and difficult to handle. This technical difficulty was overcome with a series of truncated 8-mer peptides (**3a-c**, Figure 2); including the truncated **3a**, a variant (**3b**) in which O-methyltyrosine was replaced with phenylalanine, and a variant (**3c**) in which O-methyltyrosine was replaced with the aliphatic residue leucine. In these truncated peptides the variable position is now position 2 and the His is now at position 7. The minimalist 6-residue variant (**4**) incorporating His and O-methyltyrosine at positions 1 and 6, respectively, and the cyclized 10-mer **5** were also synthesized to investigate the role of folding on catalytic function. The 6-mer is expected to be less well folded than the 8-mer due to loss of two H-bonds, and the cyclized 10-mer prevents end-fraying and should approximate a fully folded beta-hairpin.[15] NMR characterization of peptides **3a**, **4**, and **5** validated these expectations (vide infra). Lastly, N-BOC-His methyl ester (Figure 2) was used as a control for baseline measure of catalytic activity.

Stoichiometric acylation, deacylation, and catalytic competence

As a first test, 2.5 mM concentrations of these peptides were reacted in acetonitrile-d3 with 5 equivalents of a non-dye variant of the reactive tag, **6**, Scheme 3. Under these conditions the peptides stoichiometrically convert to a single isomer of the *N*-acylated product, the rate of this process being measurable by ^{1}H NMR spectroscopy. As Figure 3 demonstrates, significant rate differences were noted for acylation of **3a**, the aliphatic analog **3c**, and the control peptide *N*-BOC-His methyl ester. Under these reaction conditions **3a** is 9-fold faster than **3c** and 21-fold faster than *N*-BOC-His methyl ester. It is thus clear that the library screen successfully selected compounds demonstrating structure dependent *N*-acylation activity.

When 100 µL of TFE-*d3* was added as a nucleophile to the N-acylated peptide **3a•MeOAc**, rapid deacylation was observed by NMR spectroscopy ($t_{½}$ < 1 min), to regenerate the neutral peptide **3a** and form the TFE ester **7** (Scheme 3). The feasibility

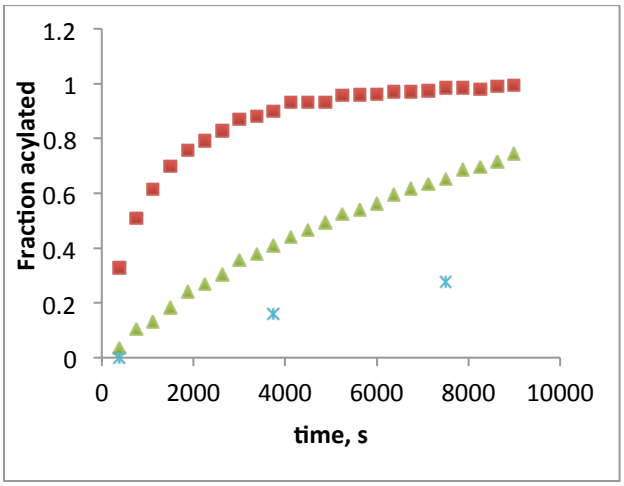

Figure 3. Stoichiometric acylation of peptide (2.5 mM) with **6** (12.5 mM) in d3 acetonitrile at 25 °C (**3a**, red squares; **3c**, green triangles; *N*-BOC His methyl ester, blue stars).

of this acyl transfer to alcohol suggests that both half reactions of the catalytic cycle are kinetically competent and multi-turnover catalysis should be possible.

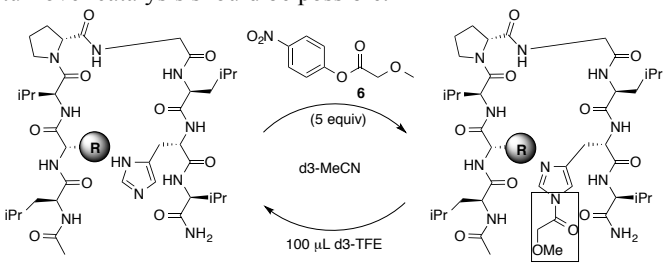

Scheme 3. Stoichiometric acylation of **3a-c** by *p*-nitrophenylmethoxyacetate (**6**) and deacylation by TFE-d3 to give **7**.

The catalytic potential of the test peptides was investigated with combinations of **6** and 25 – 100 mol% of the catalyst in trifluoroethanol-d3 (eq 1), with TFE serving as both solvent and nucleophile. The course of the conversion of **6** to **7** was conveniently monitored by ^{1}H NMR or UV-vis spectroscopy (320 nm), with relative rate data for the candidate catalysts obtained from initial rates (Table 1). The 8mer peptide **3a** with O-methyl tyrosine cross-strand from histidine displayed the highest activity relative to the control, BOC-His methyl ester, and to **3c**, the leucine-bearing 8mer peptide. Under the indicated conditions, **3a** provides a V_{rel} of 18,000 relative to background. Since the *N*-acyl intermediate does not build up during catalysis one can also calculate a second order rate constant for the turnover-limiting reaction of **3a** with **6**. Comparing this k_{cat} to the 2nd order rate constant obtained for the background reaction of **6** and d3-TFE (k_{uncat}) gives a k_{cat}/k_{uncat} of ~1x10^8 (Table 1). As the *N*-acyl intermediate does not build up during catalysis, the rate acceleration for catalyst deacylation must be even larger.

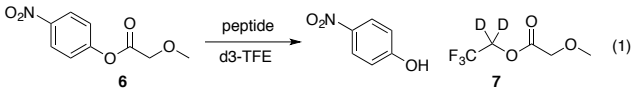

Peptide **3b**, which lacks a para-methoxy-group, is less active than **3a**, and when the aromatic residue has been replaced with leucine (**3c**), the catalyst is even less reactive. The poorly folded 6-mer **4** was also less reactive than **3a**, but more reactive than the cross-strand phenylalanine **3b**, consistent with a significant para-methoxy effect on rate. The lower reactivity of

Table 1. Initial and relative rates for peptide-catalyzed trifluoroethanolysis of **6** as determined by NMR spectroscopy.[a]

peptide	$v_{initial}$ mM/s	V_{REL} [a]	k M^{-1} s^{-1}	k_{REL}
background	4.0 E-07	1	3.4 E-9	1
BocHisOMe	1.6 E-04	400	7.1 E-03	2.1 E+06
3a	7.1 E-03	18,000	3.2 E-01	9.4 E+07
3b	2.3 E-03	5,800	1.0 E-01	3.0 E+07
3c	9.2 E-04	2,300	4.1 E-02	1.2 E+07
4	2.6 E-03	6,500	1.2 E-01	3.4 E+07
5	1.8 E-03	4,500	8.0 E-02	2.4 E+07

[a] 2.5 mM catalyst, 9 mM substrate in d3 TFE 25 °C.

the cyclic 10-mer **5**, despite being more folded (vide infra), may be attributed to steric hindrance of the histidine by the nearby disulfide linkage, which resides on the same face of the hairpin.

To rule out unusual aggregation effects on the catalyst efficiencies, kinetic measurements were performed to determine the order in catalyst. A UV-Vis assay conveniently allowed the catalyst concentrations to be varied from 0.025 mM to 0.1 mM for **3a** (8mer) and **4** (6mer). In each case the reactions were first order in peptide catalyst (Figure S1), which is consistent with a monomeric catalyst.

Catalyst characterization by NMR

Having demonstrated that peptide **3a** is a competent acyl transfer catalyst, we wished to probe the structural basis for its high activity. Our working mechanism for acyl transfer involves nucleophilic attack of the histidine onto active ester **6** to transiently generate a methoxy-acyl-imidazolium ion intermediate (**Hcat•MeOAc**$^+$), which can deprotonate to the *N*-acyl imidazole intermediate (**cat•MeOAc**).[16] Subsequent reaction of **Hcat•MeOAc**$^+$ or **cat•MeOAc** with TFE gives **7** and regenerates the catalyst **Hcat** (Scheme 4).

Scheme 4

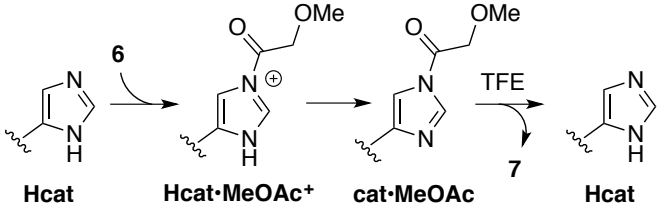

This mechanistic hypothesis was probed by characterizing several **3a** derivatives that are proposed intermediates, or models thereof (Scheme 4). In addition to **3a** itself, a model for **cat•MeOAc** was obtained by the stoichiometric acetylation of **3a** to give **3a•Ac**, while a model for **Hcat•MeOAc**$^+$ was generated by protonating **3a** with TFA to give **3a•H**$^+$. In their aggregate, the obtained NMR structural data show the gross hairpin structures to be unaffected by the **3a**, **3a•H**$^+$, and **3a•Ac** changes. What does change as the His residue is varied, however, is the conformation of this side-chain relative to others, as described below.

Global structural information was obtained on the folding states of **3a**, **4•H**$^+$, **5•H**$^+$, **3a•H**$^+$, and **3a•Ac** from 2D NMR spectra (TOCSY and NOESY) in acetonitrile-d3 and TFE-d3.[17] Alpha proton chemical shift deviations from random coil values for all peptides were consistent with a beta-hairpin, with significant negative deviation for the turn sequence (dPro-Gly) and positive shifts of > 0.1 ppm for the beta strand residues[18] except histidine, which is shielded by the cross-strand aromatic residue (Figure S2). NH shifts also demonstrated the correct H-bonding patterns between the strands, indicating correct strand registry.[19] As expected, the truncated peptide **4•H**$^+$ is less well folded than **3a•H**$^+$, whereas the cyclic peptide **5•H**$^+$ is more folded, particularly at the termini (Figure S2, S4 and S5). Importantly, no significant difference in the alpha-proton chemical shifts was observed for **3a**, **3a•H**$^+$, and **3a•Ac**, indicating that the backbone folding is similar for all three (Figure S7).

The role of the aromatic residue on the structure of **Hcat** was investigated through NMR studies on **3a**, **3b**, and **4**. Generally speaking, it was found that stronger cross-strand interactions were present in the best catalysts. Since the degree of shielding of the imidazole δ CH reports on its proximity to the face of an aromatic ring, this signature was used to assess the degree of cross strand His/aromatic interaction in the ground state structures (Figure 4a). In TFE-d3, cross-strand aromatic sidechains shield the imidazole δ CH in **3a** and **3b** (-0.23 ppm and -0.21 ppm, respectively) but not in **4** (-0.05 ppm), Table 2.[9] Shielding of the δ CH is also consistent with a T-shaped interaction of one aromatic sidechain with another, and has been seen in cross-strand interactions between phenylalanines on the nonhydrogen-bonded face of a beta hairpin.[9,10,20] The lack of CH shielding in the less reactive (and less folded) **4**, suggests that a cross-strand CH-pi interaction may be a distinguishing feature of the best catalysts (**3a**, **3b**). The cyclized peptide **5** also exhibits a shielded imidazole δ CH similar to **3a** (Table 2).

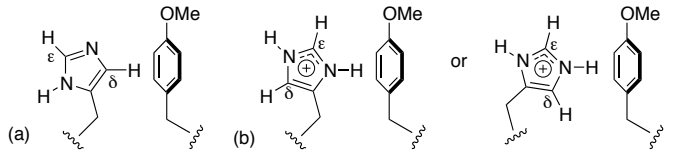

Figure 4. Possible His-π interactions in **3a** (a) and **3a•H**$^+$ (b).

Table 2. Chemical shift changes for the imidazole δ CH and the MeY methyl group upon protonation of His in TFE-d3.

Peptide	Imidazole δCH (ppm)		MeY methyl (ppm)
	X-3c	X•H$^+$-3c•H$^+$	X•H$^+$ - X
3a	-0.23	-0.08	0.08
3b	-0.22	-0.11	NA[a]
3a•Ac[b]	-0.16	NA[a]	NA[a]
4	-0.05	-0.08	0.01
5	-0.23	-0.22	0.05

a. NA = not applicable; b. in CD_3CN.

Comparison of the His δ CH in protonated versus neutral species also informed on the structure dependent role of His-aromatic interactions in a model intermediate. Interestingly, protonation of His causes a loss of upfield shifting in the imidazole δ CH of peptides **3a** and **3b**, but not **4** or **5**. This suggests that upon protonation the sidechain reorients in a manner that disrupts the ground state CH-π interaction. One intriguing possible reason for this change in geometry is that in TFE, which is a poor H-bond acceptor, the HisH$^+$ reorients to form an NH$^+$-π interaction in preference over the CH-π interaction (Figure 4b). Unfortunately the NH is invisible by NMR, so that this possibility cannot be confirmed. Nonetheless, both rotamers in Scheme 4b would provide less upfield shifting

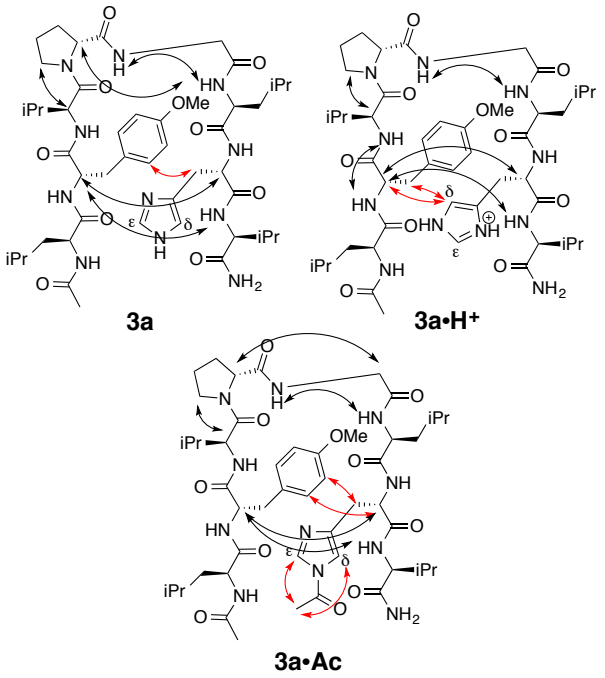

Figure 4. NOESY contacts in neutral, protonated and acylated **3c** in CD_3CN. The contacts in red represent important structural defining close contacts.

for the δ C-H. In the case of **4**, the CH-pi interaction is weak in both the protonated and nonprotonated forms. When the peptide is locked in the folded state, as in **5**, the CH-π interaction is maintained in both states, presumably because the sidechains cannot reorient in this less flexible framework.

Additional evidence for a protonation state dependent side chain orientation comes from NOE data indicating that the δ protons of His are in close proximity to the α and β protons of MeTyr in **3a•H**$^+$, but not **3a**. Peptide-dependent changes in the protonated species were also apparent in the shifting of the tyrosine O-methyl group (Table 2). Relative to their unprotonated states, **3a•H**$^+$ experiences a change in OCH_3 chemical shift upon imidazole protonation (Δδ= 0.08 ppm), whereas the change is negligible for the truncated 6-mer **4•H**$^+$ (Δδ= 0.01 ppm), and somewhat attenuated for **5•H**$^+$ (Δδ= 0.05 ppm).[21] These data suggest the feasibility of a stabilizing $HisH^+$-O interaction with MeY.

Analysis of the ^{1}H NMR spectrum of **3a•Ac** provides insight into the structure and reactivity of the putative **cat•Ac** intermediate. Distinct resonances for both components in mixtures of **3a** and **3a•Ac,** indicate that intermolecular exchange of the acyl groups does not occur on the NMR timescale. Diagnostic crosspeaks in the NOESY spectra (Figure 4), unequivocally reveal that imidazole is *N*-acylated at the ε nitrogen. Peptide **3a•Ac** also displays new NOE crosspeaks that correspond to close contacts between the histidine α and β protons and the aromatic ring of O-methyl tyrosine (Figure 4), suggestive of a conformation that is more similar to **3a** than **3a•H**$^+$, but not identical (note the His β protons exhibit NOEs to different MeY ring positions in **3a** and **3a•Ac**). Furthermore, upfield shifting of the δ CH on His is intermediate to that of **3a** and **3a•H**$^+$ (Table 2). Otherwise the structure of **3a•Ac** as determined by 2D NMR is largely unchanged versus **3a** (see Figure S7). Lastly, an intermediate degree of upfield shifting of the δ CH of His was observed when acylated (-0.16 ppm) relative to **3a** or **3a•H**$^+$. This implies that the CH-π interaction is maintained, although either less populated or with a slightly different orientation than for **3a**, as suggested by the NOEs.

In each of the catalyst intermediates or their models, it is clear that the His modification adopts a unique side chain orientation, utilizing cross strand interactions to benefit as needed. This strategy delineates an intriguing mechanism for the catalyst to stabilize a series of transiently populated intermediates on progressing along a multi-intermediate catalytic reaction coordinate.

Discussion and Conclusions

The employment of a reactive tagging scheme that incorporates a dye-modified active ester to screen a solid phase library of beta hairpin peptides has led to a hit peptide incorporating an aromatic residue containing a heteroatom (O-methyltyrosine preferred) cross-strand from histidine. A slightly shortened more soluble version of the hit, peptide **3a**, is rapidly acylated with **6**, demonstrating the viability of the solid phase screen for selecting a competent nucleophile from the library. The resulting acylated peptide **3a•MeOAc** is also rapidly deacylated by trifluoroethanol-d3, effectively closing a catalytic cycle of a nucleophilic catalytic mechanism. Indeed, when the reaction was carried out in trifluoroethanol-d3, **3a** was found to be the most reactive catalyst for the conversion of **6** to **7**, achieving a V_{rel} of nearly 18,000 over background and 43-fold over a control His-containing peptide. When expressed as a ratio of second-order rate constants (k_{rel}), the magnitude of the rate acceleration for **3a** was significant ($9.4x10^7$, Table 1). Truncated and cyclized variants, as well as mutants that remove either the methoxy group or the aromatic sidechain in its entirety helped to localize the origin of the enhanced reactivity to the cross-strand imidazole-aromatic interface.

The observation that even the control peptide **3c**, which positions a leucine instead of an aromatic sidechain across strand from the reactive histidine, is more active than the baseline control compound boc-histidine methyl ester, suggests that the beta-hairpin scaffold is inherently able to eliminate nonproductive, sterically obstructed conformers and thereby enhance activity.

Peptides that were less folded than **3a** (6-mer **4**) and more constrained (cyclic **5**) were both less active. The former being considerably less structured and thus less preorganized, while the latter was better folded, but also less flexible and possibly also more hindered. The collection of data thus indicate that hit peptide **3a** utilizes a balanced combination of flexibility and organization together with a means for stabilizing developing charge in the nucleophilic imidazole to increase its nucleophilicity and/or its population of reactive conformers.

How might a cross-strand His-aromatic interaction enhance catalytic activity? Reasonable suggestions based on our NMR

studies include an imidazole-directing function for the aromatic sidechain, an enhancement of imidazole nucleophilicity by a CH-π (in the ground state) or a cation-π interaction (in the transition state),[22] or both. His CH-π interactions have been observed to influence folding and reactivity in peptides and proteins, such as an i/i+4 aromatic/histidine stabilizing effect in alpha-helices, and the pH modulating effect of aromatic residues in Barnase, both of which are thought to be modulated by CH-π and cation-π interactions.[23] This also parallels the significant contribution of CH-π and cation-π interactions to the design of many organocatalysts.[24] These results are also reminiscent of the catalytic function of the active site tryptophan in the enzyme liver epoxide hydrolase.[25]

Evidence for reactivity-enhancing aromatic-His cross-strand interactions emerged from examination of the imidazole chemical shifts in the model peptides. In comparison to the peptide with a cross-strand aliphatic group (**3c**), peptides **3a** and **3b** display substantial changes in the chemical shift of the His δ CH due to shielding by the aromatic ring. These upfield shifts are consistent with population of a structure that has the cross-strand His and aromatic groups interacting in an edge-face geometry. The less reactive, less folded peptide **4** does not exhibit as much upfield shifting. Protonation or acylation of **3a** results in differing degrees of shielding of the His δ CH, suggesting subtle changes in conformation in these models of reactive intermediates. Peptides carrying aromatic methoxy substituents also experienced a small downfield shift for the *O*-methyl group when the His is protonated, consistent with its influence on catalytic activity. The beneficial effect of the OMe group in **3a** is presumed to result from an additional stabilizing interaction provided by the oxygen lone pairs directly, or by enhancing the strength of the key aromatic interactions through an additive dipole-dipole interaction.[26] The downfield shift of the O-methyl group is more pronounced for peptide **3a** than the truncated peptide **4** or disulfide-bridged cyclic peptide **5**, suggesting a subtle interplay between the ability of the structure to adopt stabilizing conformations and the flexibility of the peptide: the 6-mer may be too conformationally flexible to obtain the optimal conformation between O-methyltyrosine and $HisH^+$, whereas the conformation restriction in **5** may preclude the optimal conformation. These results are consonant with the findings of Miller, et al., who similarly observed that rigidification of a beta-hairpin catalyst via cyclization had a deleterious effect on reactivity and selectivity.[27]

Taken together these data suggest that as the catalyst proceeds along the reaction coordinate, each intermediate and (presumably) transition state can be stabilized by relatively precise structural minima. Moreover, the structural perturbations needed to achieve this phenomenon are localized in the side chains as the gross features of the beta-hairpin are largely unchanged from compound to compound.

Also emerging from the data is a likely role of aromatic His interactions in stabilizing developing positive charge on the histidine. Although it is not yet clear whether the key noncovalent interactions occur in the ground state to properly position a nucleophilic histidine (CH-pi) or in the transition state as charge is developed (cation-pi), or both, it is clear that these interactions are important in distinguishing these catalysts from the others during the screen.

What therefore emerges from the sum of these data is a model for catalysis that relies on conformationally flexible side chain groups and arrays of noncovalent interactions to stabilize transient structures. Preorganization, flexibility, and accessibility to a network of non-covalent interactions therefore emerge as themes with clear biomimetic parallels.

Experimental

Library synthesis

A solid phase peptide library was synthesized using a split-and-mix methodology. 1 g Tentagel S NH_2 (130 micron, 0.29 meq/g loading) was swelled in DCM. 330 mg Fmoc- photolabile linker (Anaspec) (2 equivalents) was coupled to the resin overnight using HCTU (240 mg) and DIPEA (200 uL) in DMF. Solid phase peptide synthesis using the Fmoc strategy was carried out. The peptide sequence was Ac-LX_1VX_2VdPGLHVVV-photolabile linker-Tentagel S. All couplings were carried out over 8 hours using HBTU/HOBt (4 equivalents) and 4 equivalents of amino acid building block and 8 equivalents of DIPEA. X_1 and X_2 were split into 10 x 100 mg portions and coupled with the following amino acid building blocks: Fmoc-valine, Fmoc-phenylalanine, Fmoc-pentafluorophenylalanine, Fmoc-O-methyltyrosine, Fmoc-4-dimethylaminophenylalanine, Fmoc-3,4-dimethoxyphenylalanine, Fmoc-tryptophan, Fmoc-homophenylalanine, Fmoc-citrulline, and Fmoc-ε-acetyllysine. Each split was recombined for deprotection and further peptide synthesis. Fmoc deblocking was carried out using 20% v/v piperidine in DMF (three fifteen minute intervals). N-terminal capping was carried out using 1:1:2 pyridine:acetic anhydride:DMF for 30 minutes. The resulting resin was washed with DMF and DCM, dried, and deprotected using 2.5% water, 2.5% TIPS and 95% TFA for two hours. The deprotected resin was washed with DCM, methanol, and DMF followed by 5% DIPEA in DCM, then DCM.

Library screening

50 mg portions of the solid-phase peptide library were subjected to **1** (10 mg/ mL) in DCM for varying time intervals in fritted polypropylene syringes. After 30 min, the **1** solution was washed away and the resin was washed repeatedly with DCM. The resulting beads were dried and spread on a plastic petri dish. A dissecting stereomicroscope and glass probes were used to pick red beads, which were placed in methanol. Peptides were cleaved from the beads using a 360 nm UV lamp overnight with stirring. The resulting methanolic solution was evaporated to produce a concentrated solution (10 μL). This residue was analyzed by MALDI FT-MS using 2,5-dihydroxybenzoic acid as matrix.

Peptide synthesis

Preparative quantities of peptides were obtained through solid-phase peptide synthesis using the Fmoc strategy on CLEAR-amide resin. Couplings were carried out over 6 hours or overnight using HBTU/HOBt with DIPEA. Fmoc deblocking was carried out using 20% v/v piperidine in DMF. N terminal acetylation was carried out with 1:1:2 pyridine:acetic anhydride:DMF for 30 minutes. Cleavage from resin was carried out with 2.5% water, 2.5% TIPS and 95% TFA over two hours. The resulting cleavage solution was evaporated under nitrogen flow. Cold diethyl ether was added, and the resulting precipitate was centrifuged at 6000 rpm. Ether was decanted and fresh ether was added, and this procedure was repeated for a total of thee centrifugations. The resulting white solid was dried, dissolved in a minimal amount of methanol, brought up in eluent A (95% water, 5% acetonitrile, 0.1% TFA) and purified by RP-HPLC using a gradient of 50% A to 0% A and methanol.

Kinetic studies in acetonitrile

Acetylation kinetics for the 8-mer peptides was investigated in d3-MeCN. Peptide concentration was 2.5 mM, with para-nitrophenylmethoxyacetate concentration of 12.5 mM and 10 mM DIPEA, with tetrachloroethane as an internal standard. 1D NMR spectra were acquired every 375 seconds using 500 MHz Bruker NMR spectrometer with a BBI probe.

Kinetic studies in TFE (NMR)

Kinetics of *para*-nitrophenylmethoxyacetate trifluoroethanolysis in TFE was investigated in d3-TFE. Peptide was titrated to neutrality using 10 μL aliquots of TEA in d3-TFE (72 mM solution). Peptide concentration was 2.5 mM, with pNPMA concentration of 9 mM. 1D NMR spectra were acquired every 375 seconds using 500 MHz Bruker NMR spectrometer with a BBI probe.

Kinetic studies in TFE (UV-vis)

Kinetics of para-nitrophenylmethoxyacetate trifluoroethanolysis in TFE was investigated in dry TFE. Parallel runs were carried out in an HP UV-Vis spectrophotometer at 320 nm. Stock solutions of catalyst were prepared by treating a methanolic solution of protonated peptide with A-21 solid phase base and filtering. The filtrate was evaporated to dryness and reconstituted with dry TFE (1 mL). A stock solution of p-nitrophenylmethoxyacetate was prepared from 10 mg p-nitrophenylmethoxyacetate in 1 mL dry TFE. Samples were run by mixing TFE (750 – 950 μL) with catalyst (25 – 200 μL) and substrate (25 mL), producing solutions that were 0.025, 0.05, and 0.1 mM in catalyst and 0.1 M in substrate.

Acknowledgements

MRG and MLW thank the Defense Threat Reduction Agency (HDTRA1-10-1-0030), and SL thanks the Army Research Office (ARO) for support. MM acknowledges a National Academies Postdoctoral Fellowship.

Notes and references

[a] *Department of Chemistry, University of North Carolina at Chapel Hill, North Carolina 27599-3290, USA*
[b] *U. S. Army Research Office, P. O. Box 12211, Research Triangle Park, North Carolina 27709, USA*

Electronic Supplementary Information (ESI) available: [details of any supplementary information available should be included here]. See DOI: 10.1039/b000000x/

1 B. Geibel, M. Merschky, C. Rether and C. Schmuck, 2012. Artificial Enzyme Mimics. *Supramolecular Chemistry: From Molecules to Nanomaterials*; R. Breslow, and S. D. Dong, *Chem. Rev.,* 1998, **98,** 1997-2011; L. Baltzer, H. Nilsson, J. Nilsson, *Chem. Rev.,* 2001, 101, 3153-3163; L. Baltzer and J. Nilsson, *Curr. Op. Biotechnology,* 2001, **12,** 355-360; Nicoll, A. J.; Allemann, R. K.; L. Baltzer, H. Nilsson, J. Razkin, *Org. Biomol. Chem.*, 2004, **2**, 2175-2180; L. Baltzer, H. Nilsson, J. Razkin, *J. Am. Chem. Soc.*, 2007, **129**, 14752-14758,; K. S. Broo, H. Nilsson, J. Nilsson, A. Flodberg and L. Baltzer, *J. Am. Chem. Soc.,* 1998, **120,** 4063-4068.

2 A. Berkessel, *Curr. Opin. Chem. Biol.,* 2003, **7**, 409-419; J. D. Revell and H, Wennemers, *Curr. Opin. Chem. Biol.,* 2007, **11,** 269-278; M. H. Fonseca and B. List, *Curr. Opin. Chem. Biol.,* 2004, **8**, 319-326; P. Krattiger, C. McCarthy, A. Pfaltz and H. Wennemers, *Angew. Chem. Int. Ed.,* 2003, **42,** 1722-1724; A. Berkessel, R. Riedl, *J. Comb. Chem.,* 2000, **2,** 215-219; H. B. Albada, R. M. J. Liskamp, *J. Comb. Chem.,*2008, **10**, 814-824; C. Schmuck, U. Michels, J. Dudaczek, *Org. Biomol. Chem.,* 2009, **7,** 4362-4368.

3 H. Wennemers, *Chem. Commun.* 2011, **47,** 12036-12041.

4 G. T. Copland and S. J. Miller, *J. Am. Chem. Soc.,* 2001, **123,** 6496-6502; S. J. Miller, G. T. Copeland, N. Papaioannou, T. E. Horstmann and E. M. Ruel, *J. Am. Chem. Soc.,* 1998, **120,** 1629-1630; S. J. Miller, *Acc. Chem. Res.* 2004, **37**, 601-610; E. A. C. Davie, S. M. Mennen, Y. Xu and S. Miller, *Chem. Rev.* 2007, **107,** 5759-5812.

5 S. Bezer, M. Matsumoto, S. J. Lee, M. L. Waters, M. Gagné, *Org. Biomol. Chem.,* 2014, **12,** 1488-1494.

6 A. Gutteridge, J. M. Thornton, *TRENDS in Biochemical Sciences,* 2005, **30**, 622-629; G. J. Bartlett, C. T. Porter, N. Borkakoti, J. M. Thornton, *J. Mol. Biol.* 2002, **324,** 105-121; C. M. Quezada, D. J. Hamel, C. Gradinaru, A. M. Bilwes, F.W. Dahlquist, B. R. Crane, M. I. Simon, *J. Biol. Chem.,* 2005, **280,** 30581-30585.

7 F. A. Syud, H. E. Stanger and S. H. Gellman, *J. Am. Chem. Soc.,* 2001, **123,** 8667-8677.

8 S. Aravinda, V. V. Harini, N. Shamal, C. Das, P. Balaram, *Biochemistry,* **43**, 1832-1846; A. G. Cochran, N. J. Skelton, M. A. Starovasnik, *Proc. Nat. Acad. Sci. USA,* 2001, **98,** 5578-5583; N. H. Andersen, K. A. Olsen, R. M. Fesinmeyer, X. Tan, F. M. Hudson, L. A. Eidenschink, and S. R. Farazi, *J. Am. Chem. Soc.,* 2006, **128,** 6101-6110; L. Eidenschink, E. Crabbe and N. H. Andersen, *Biopolymers*, 2009, **91**, 557–564.

9 R. Mahalakshmi, S. Raghothama, and P. Balaram, *J. Am. Chem. Soc.,* 2006, **128,** 1125-1138; R. Mahalakshmi, G. Shanmugam, P. L. Polavarapu, and P. Balaram, *ChemBioChem,* 2005, **6**, 2152-2158.

10 C. D. Tatko and M. L .Waters, *J. Am. Chem. Soc.,* 2002, **124**, 9372-9373; C. D. Tatko, and M. L. Waters, *J. Am. Chem. Soc.,* 2004, **126**, 2028–2034.

11 T. S. Haque and S. H. Gellman, *J. Am. Chem. Soc.,* 1997, **119**, 9, 2303-2304; H. E. Stanger and S. H. Gellman, *J. Am. Chem. Soc.,* 1998, **120**, 17, 4236-4237.
12 K. S. Lam, M. Lebl, and V. Krchnak, *Chem. Rev.,* 1997, **97**, 411-448;
13 H. De Muynck, A. Madder, N. Farcy, P. J. De Clerq, M. N. Perez-Payan, L. M. Ohberg, *Angew. Chem. Int. Ed.,* 2000, **39,** 1, 145-148; A. Madder, L. Li, H. De Muynck, N. Farcy, D. Van Haver, F. Fant, G. Vanhoenacker, P. Sandra, A. P. Davis and P. J. De Clerq, *J. Comb. Chem,* 2002, **4**, 552-562.
14 A. Madder, N. Farcy, N. G. C. Hosten, H. De Muynck, P. J. De Clercq, J. Barry, A. P. Davis, *Eur. J. Org. Chem.,* 1999, 2787-2791.
15 S. J. Russel and A. G. Cochran, *J. Am. Chem. Soc.,* 2000, **122**, 12600-12601; A. G. Cochran, R. T. Tong, M. A. Starovasnik, E. J. Park, R. S. McDowell, J. E. Theaker, and N. J. Skelton, *J. Am. Chem. Soc.,* 2001, **123,** 4, 625-632.
16 T. C. Bruice, G. L. Schmir, *J. Am. Chem. Soc.,* 1957, **80,** 148-156.
17 see SI for details
18 S. R. Griffith-Jones, A. J. Maynard, M. S. Searle, *J. Mol. Biol.* 1999, **292,** 1051-1069.
19 R. M. Fesinmeyer, F. M. Hudson, K. A. Olsen, G. W. N. White, A. Euser, N. H. Andersen, *J. Biomolecular NMR,* 2005, **33,** 213-231..
20 C. D. Tatko, M. L. Waters, *Org. Lett.,*2004, **6,** 3969-3972.
21 C. Zhao, P. L. Polavarapu, C. Das, and P. Balaram, *J. Am. Chem. Soc.,* 2000, **122**, 8228-8231.
22 S. K. Awasthi, S. Raghothama, P. Balaram, *Biochem. Biophys. Res. Commun.,* **1995, 216,** 375-381; M. Ramirez-Alvarado, F. J. Blanco, L. Serrano, *Nature Struct. Biol.* 1996, **3***,* 604-612; A. J. Maynard, G. J. Sharman, M. S. Searle, *J. Am. Chem. Soc.* 1998**, 120***,* 1996-2007.,
23 D. A. Dougherty, *Acc. Chem. Res.,* 2013, **46** (4), 885; N. Zacharias and D. A. Dougherty, *TRENDS in Pharmacological Sciences,* 2002, **23**, 6, 281.
24 E. J. Corey, T.-P. Loh, T. D. Roper, M. D. Azimiora, and M. C. Noe, *J. Am. Chem. Soc.,* 1992, **114,** 8290-8292; T. Kawabata, M. Nagato, K. Takasu, and K. Fuji, *J. Am. Chem. Soc.,* 1997, **119,** 3169-3170; S. J. Miller, G. T. Copeland, N. Papaioannou, T. E. Horstmann and E. M. Ruel, *J. Am. Chem. Soc.,* 1998, **120,** 1629-1630; for a review on cation-p interactions in organocatalysis, see S. Yamada and J. S. Fossey, *O. Biomol. Chem.,* 2011, **9**, 7275.
25 J. Fernandez-Recio, A, Vazquez, C. Civera, P. Sevilla, and J. Sancho, *J. Mol. Biol.,* 1997, **267**, 184- 197; R. Loewenthal, J. Sancho, and A. R. Fersht, *J. Mol. Biol.,* 1992, **224**, 759-770.
26 D. Bromme, P. R. Bonneau, E. Purisimia, P. Lachance, S. Hajnik, D. Y. Thomas, and A. C. Storer, *Biochemistry,* 1996, **35,** 3970-3979; M. A. Argiriadi, C. Morisseau, B. D. Hammock, and D. W. Christianson, *Proc. Natl. Acad. Sci. USA*, 1999, **96**, 10637-10642.
27 E. R. Jarvo, G. T. Copeland, N. Papaioannou, P. J. Bonitatebus, Jr., and S. J. Miller, *J. Am. Chem. Soc.,* 1999, **121**, 11638-11643.